In Situ and Real-Time Visualization of Mechanochemical Damage in Double-Network Hydrogels by Prefluorescent Probe via Oxygen-Relayed Radical-Trapping

Yong Zheng[1‡], Julong Jiang[2‡], Mingoo Jin[1,3]*, Daiyo Miura[3], Fei Xue Lu[4], Koji Kubota[1,3], Tasuku Nakajima[1,5], Satoshi Maeda[1,2]*, Hajime Ito[1,3]*, Jian Ping Gong[1,5]*

[1]Institute for Chemical Reaction Design and Discovery (WPI-ICReDD), Hokkaido University, Sapporo 001-0021, Japan.

[2]Department of Chemistry, Faculty of Science, Hokkaido University, Sapporo 060-8628, Japan.

[3]Division of Applied Chemistry, Graduate School of Engineering, Hokkaido University, Sapporo 060-8628 Japan.

[4]Graduate School of Life Science, Hokkaido University, Sapporo 001-0021, Japan.

[5]Faculty of Advanced Life Science, Hokkaido University, Sapporo 001-0021, Japan.

ABSTRACT: Visualization of mechanochemical damages especially molecular-scale bond scission in polymeric materials is of great industrial and academic significance. Herein, we report a novel strategy for in situ and real-time visualization of mechanochemical damages in hydrogels by utilizing prefluorescent probe via oxygen-relayed free-radical trapping. Double-network (DN) hydrogels that generate numerous mechanoradicals by homolytic bond scission of the brittle first network at large deformation are used as model materials. Theoretical calculation suggests that mechanoradicals generated by the damage of the first network undergo an oxygen-relayed radical transfer process which can be detected by the prefluorescent probe through radical–radical coupling reaction. Such an oxygen-relayed radical-trapping process of prefluorescent probe exhibits a dramatically enhanced emission, which enables the real-time sensing and visualization of mechanochemical damages in DN hydrogels made from brittle networks of varied chemical structures. To the best of authors' knowledge, this work is the first report utilizing oxygen as a radical-relaying molecule for visualizing mechanoradical damages in polymer materials. Moreover, this new method based on the probe post-loading is simple and does not introduce any chemical structural changes in the materials, outperforming most previous methods that require chemical incorporation of mechanophores into polymer networks.

1. Introduction

Visualization of mechanochemical damages in polymeric materials including elastomers and gels is of great significance in both applications and fundamental studies, such as internal damage sensing and fracture mechanism analysis.[1, 2] The fracture of polymeric materials often couples a wide range of length scales ranging from molecular-scale bond scission (mechanochemical damage), microscale localized small cracks to macro-crack damage. The polymeric materials are usually designed to be as robust as possible for practical applications, but they are susceptible to catastrophic global failure once the nanoscale mechanochemical damages lead to the microscale localized cracks, which further percolate to macro-cracks. Although in relatively large scale, the macro-crack damage could be easily observed by optical microscopy, the detection and visualization of molecular-scale mechanochemical damages, which are precursors of macroscopic failures, still pose a critical challenge in the related field. Therefore, it is always desirable to develop methods that could reveal mechanochemical damages in polymeric materials, especially for the molecular-level bond scission prior to the catastrophic material fracture.

For this purpose, a variety of mechanophores producing mechanochromic or mechanoluminescent responses have been applied to characterize the mechanochemical damages in polymeric materials.[1-7] For example, by chemically introducing mechanophores into the polymer backbones or the cross-linker units, mechanochemical damages of the mechanophores can be detected by the mechanochromism or mechano-induced chemiluminescence.[7] This protocol allows the detection of the localized stress concentration. Otsuka and co-workers incorporated diarylbibenzofuranone (DABBF) mechanophore in the polymer main chain for polyurethane elastomers. Under the mechanical force, the DABBF mechanophore breaks into two stable carbon-centered radicals, that is, a process accompanied by a large shift in light absorbance from 346 nm to 650 nm, which enables the visualization of mechanochemical damages (**Figure 1a(i)**).[3] Creton and co-workers have developed a strategy to visualize the spatially resolved sacrificial bond breakage using a chemoluminescent cross-linker, named bis(adamantyl)-1,2-dioxetane bisacrylate (BADOBA), in multiple-network elastomers.[6] Under the external force, the dioxetane group would break into two adamantanone units, one of which is in the excited state which will later get relaxed to the ground state by emitting a photon in the bright blue range of the spectrum (**Figure 1a(ii)**). In a more recent report, Creton and co-workers have also incorporated a fluorogenic mechanophore into the multiple-network elastomers as the crosslinker unit based on a Diels-Alder adduct of π-extended anthracene (**Figure 1a(iii)**).[1, 2] In its native form, the mechanophore is non-fluorescent; when subjected to force, the mechanophore scission occurs to release a fluorescent π-

extended anthracene moiety, therefore enabling the spatially resolved visualization of mechanochemical damages in the materials. However, chemically incorporating the mechanophores into the polymer backbones or cross-linker units has some limitations: (1) the mechanophores are usually activated at a smaller force than that of chemical bonds in the original polymer, which could possibly change the intrinsic fracture behavior of the material to some extent[8-10]; (2) it requires specific chemical synthesis for the materials of interest, which therefore limits the broad application.

An alternative strategy to reveal the mechanochemical damage is to detect mechanoradicals formed from the polymer network. More specifically speaking, the mechanochemical damages of polymeric materials are often caused by homolytic bond scission of polymer chains, which eventually lead to the formation of free radicals (so-called mechanoradicals[11-13]) at the broken ends of molecules. The challenge of this strategy is that the mechanoradicals are usually short-lived, making them difficult to be detected even using special equipment such as electron spin resonance (ESR)[14-16]. Facile and universal chemical methods to visualize the mechanoradicals in polymer materials are in great demand.

Gong and coworkers recently reported a method to visualize the mechanochemical damage in double-network (DN) hydrogels via the mechanoradical polymerization (**Figure 1b**).[17] The DN hydrogels, featured by contrasting double network structures, are typically consisting of a densely cross-linked stiff and brittle first network and a sparsely cross-linked soft and stretchable second network.[18,19] Owing to the contrasting network structure, massive mechanoradicals (estimated as ~ 10 μM) could be generated by the cleavage of the stiff and brittle first network strands under mechanical loading while the whole integrity of the material could be maintained by the soft and stretchable second network without causing global material failure.[20] To visualize the mechanoradicals, monomers were pre-loaded in the DN hydrogels. When mechanoradicals are generated, they subsequently trigger the following polymerization of monomers to form a temperature-responsive polymer poly(*N*-isopropylacrylamide) (PNIPAm). In the meantime, a fluorescent molecule, 8-anilino-1-naphthalenesulfonic acid (ANS), that exhibits strong fluorescence in the hydrophobic environment was used to detect PNIPAm at high temperature. This method enables visualization of internal local damage in DN hydrogels but meanwhile has some limitations: (1) as the mechanoradical concentration is much lower than that of the oxygen dissolved in hydrogels (~200 μM)[21], the mechanical testing must be performed on the deoxygenated samples to avoid the quenching of mechanoradicals by oxygen; (2) it is not able to visualize the fracture process *in situ* on a real-time basis, since the fluorescence observation should be performed after the polymerization and at an elevated temperature.[17]

Recently, fluorescent probes have been used to detect the polymer chain scission caused by the ball milling of polymer powders. The fluorescence can be realized by the reaction between the probe and the mechanoradicals generated from the polymer. For example, Otsuka and co-workers have reported that, the unstable mechanoradicals generated from polystyrene can undergo a hydrogen-atom transfer (HAT) reaction with diarylacetonitrile to form the stable diarylacetonitrile radicals, which exhibit a yellow fluorescence under the UV irradiation.[22] Diesendruck and co-workers have reported that pyrenyl nitrone could be utilized as a radical-trapper for the detection of mechanoradicals in solutions through spectroscopic measurements.[23] Ito and co-workers have reported that the luminescent polymeric materials could be directly prepared from generic polymers via force-mediated mechanoradical coupling with a prefluorescent reagent **P**.[24] More specifically, the prefluorescent reagent **P**, which bears a nitroxide radical (2,2,6,6-tetramethylpiperidine 1-oxyl (TEMPO) moiety) tethered to coumarin-based luminophore, shows a weak fluorescence in the original state due to the quenching of the excited state.[25] However, when the nitroxide radicals couple with other free radicals, **P** can show a strong fluorescence emission from the coumarin-based luminophore.[24]

In this work, we intend to develop an *in-situ* and real-time visualization method to detect the mechanochemical damage in bulk hydrogel materials by utilizing the fluorescent probes under open air conditions. We chose the radical-trapping prefluorescent probe **P** as the model probe and the DN hydrogels that produce large number of mechanoradicals as the model hydrogel material (**Figure 1c**). Specifically, under the external stretching force, bond scissions occurring in the overstressed polymer chains can produce mechanoradicals in the mechanochemical damage region. These short-lived mechanoradicals can either directly react with the pre-loaded prefluorescent molecule **P** via the mechanoradical coupling reaction (the reaction pathway **1** shown in **Figure 1c**), or undergo an oxygen-relayed radical transfer reaction pathway **2** to amplify the probability of radical coupling reaction with **P**. Following this protocol, the mechanochemically damaged region would exhibit a strong fluorescence emission so that mechanochemical damage in the materials could be easily detected and visualized.

We first synthesized a series of DN hydrogels with the varied chemical structures for the first network. Theoretical calculations were conducted to predict the bond cleavage positions in the brittle first networks and meanwhile to confirm that the bond scissions in these networks are based on homolytic cleavage. Furthermore, our calculation results suggest that it has a low barrier or even barrierless for the radical-radical coupling reaction between the prefluorescent molecule **P** and these mechanoradicals, which ensures the proposed probing mechanism **1**. Our calculation also revealed a possible oxygen-relayed radical transfer process **2**, which is expected to increase the probability for the radical-probe coupling reaction. Following the suggestions provided by DFT calculations, we then experimentally confirmed that the reaction mechanism **2**, rather than mechanism **1**, plays a predominant role under ambient conditions. Finally, we demonstrated the experimental outcomes of the *in-situ* and real-time visualization of the mechanochemical damages in hydrogels under ambient conditions. It has to be noted that, generally, oxygen is considered to have a negative effect as it could terminate radical reactions[26-28]. It therefore greatly restricts the usage of mechanoradicals.[17] However, a very recent work demonstrated the positive role of oxygen, as it can promote an unusual atom transfer radical polymerization.[29] To our surprise, oxygen was also found to play a positive role in promoting the luminescence in our work. To the best of our knowledge, this is the first report utilizing oxygen as a radical relayer for visualizing mechanoradical damages in polymeric materials.

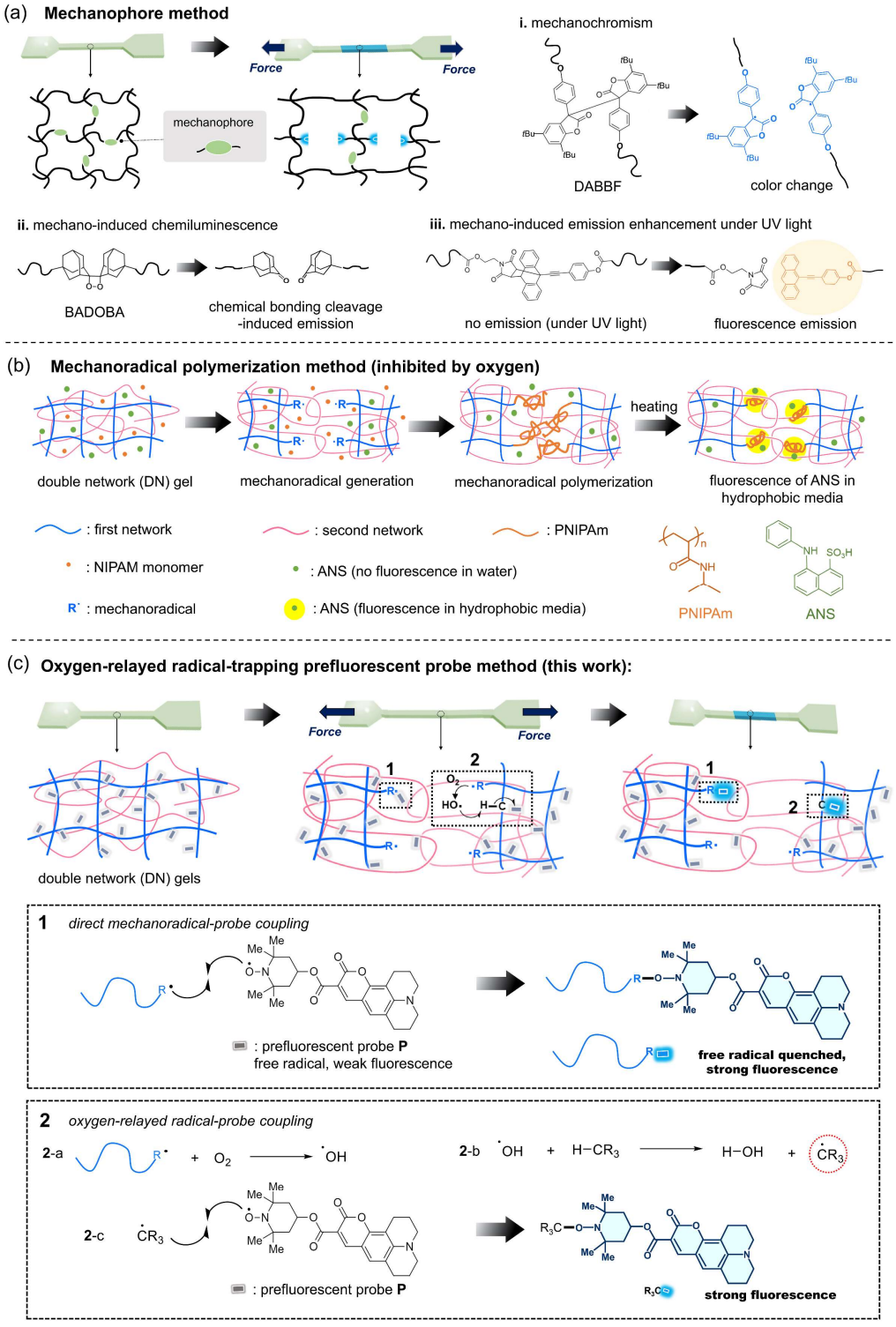

Figure 1. Schematic illustrations of the differences between the previously reported methods and the method developed in this work to visualize the mechanochemical damage in polymeric materials. (a) reported mechanophore method that covalently inserting mechanophores into polymeric materials;[1-3, 6] (b) reported mechanoradical polymerization method in which a thermally sensitive polymer PNIPAm is incorporated to the network by mechanoradical-triggered polymerization and is then detected by a fluorescent molecule ANS;[17] Reproduced from ref [17]. Copyright 2020 American Chemical Society. (c) proposed oxygen-relayed radical-trapping prefluorescent probe method utilizing a prefluorescent reagent **P** that couples with radicals formed through an oxygen-relayed pathway starting with the mechanoradicals.

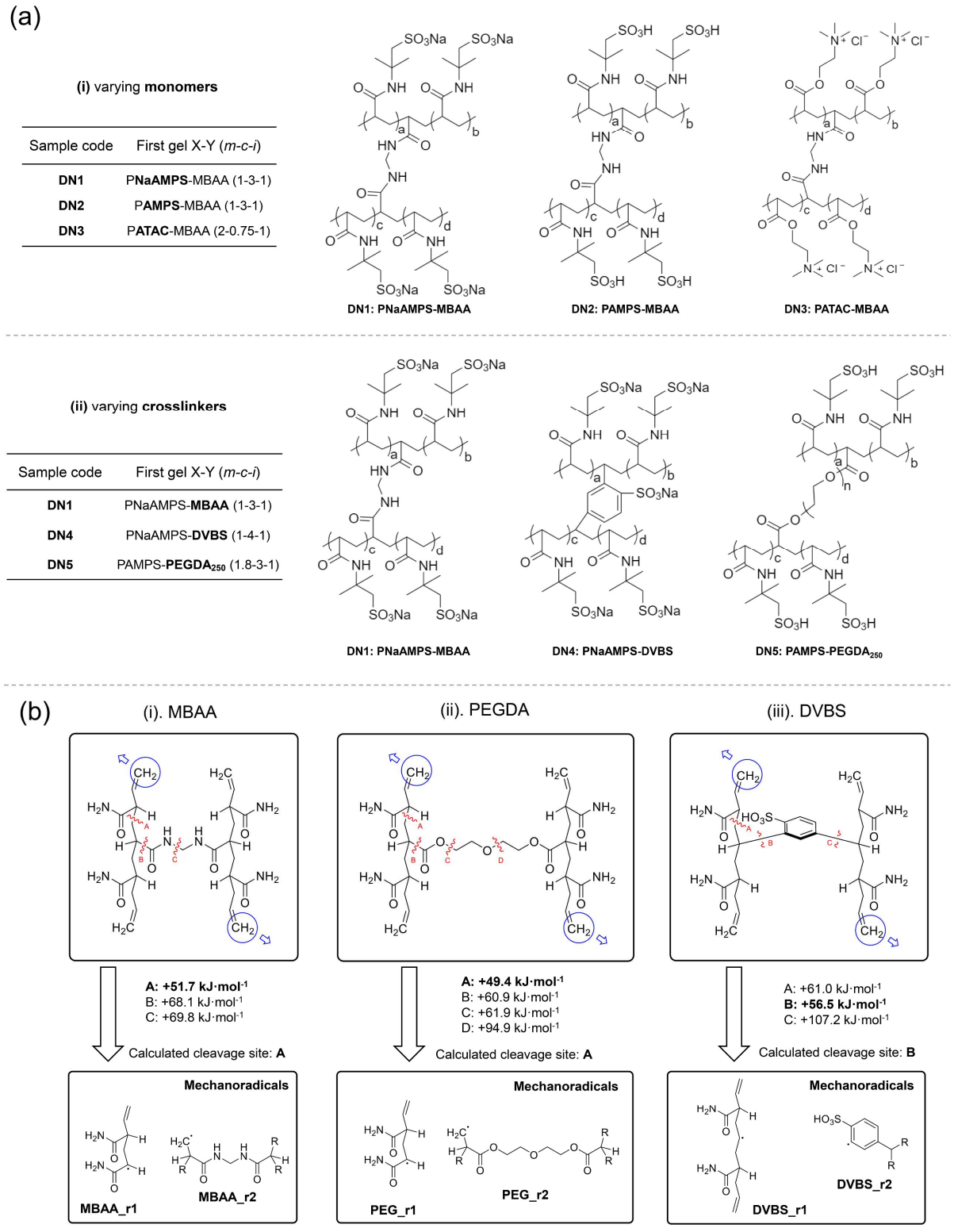

Figure 2. (a) The sample code of various DN gels with varied first network structure synthesized from various monomers (i) and crosslinkers (ii), and the corresponding chemical structure for the first network. (b) Plausible cleavage patterns considered in our AFIR calculations (blue circles and arrows indicate the fragments where a repulsive force of 4000 pN is added). Computed free energy barriers (UB3LYP-D3/Def2SVP level) of bond homolysis at different cleavage sites at F = 4000 pN are shown in the figure.

2. Results and Discussion

Density function theory (DFT) simulation. Density function theory (DFT) simulation of the bond rupture, mechanoradical-probe coupling reaction and oxygen-relayed radical transfer in DN gels were considered in our study first. Generally, mechanoradicals in DN gels are generated by the rupture of the stiff and brittle first network under mechanical loading on the sample.[17, 20] Thus, the variety of mechanoradical generations should be determined by the structure of the first polymer network (*e.g.*, the monomers and the crosslinkers).[30] To examine the generality of our concept, five types of DN gels which possess the same second PAAm network but different first network structure from varied monomers and crosslinkers were carefully synthesized by us (**Figure 2a**). Among them, 2-acrylamido-2-methylpropane sulfonic acid sodium salt (NaAMPS), 2-acrylamido-2-methyl-1-propanesulfonic acid (AMPS), and 2-(acryloyloxy)ethyl trimethylammonium chloride (ATAC) were used as monomers (SI, **Figure S1a**); *N*, *N'*-methylenebis(acrylamide) (MBAA), 2,4-divinylbenzenesulfonic acid sodium salt (DVBS), poly(ethylene glycol) diacrylate ($PEGDA_{250}$; number average molecular weight M_n 250) were used as crosslinkers (SI, **Figure S1b**). Taking DN1 as a typical example, it was prepared to have the first network as PNaAMPS-MBAA, whose monomer and crosslinker are NaAMPS and MBAA, respectively.

Concerning the effect of various crosslinkers, we first simulated the force-promoted bond rupture process for these DN gels which possess different first networks by the artificial force induced reaction (AFIR) method. It is known that the AFIR method has been widely used for the mechanistic exploration of organic reactions.[31] Here, an extended AFIR method was employed to study the reactions under stress.[24, 30, 32] In such calculations, two sets of forces are used simultaneously to simulate a mechanochemical reaction under stretching force. More specifically, a repulsive force F_τ was explicitly added between the certain fragments of a model network molecule to simulate the tensile force that the polymer network experiences in the experiment. Meanwhile, another set of force, which is a pure artificial force, was employed to the specific covalent bonds to trigger the homolytic bond cleavage. The detailed descriptions of our DFT calculation are included in SI. Note that the -NHR groups on the PAMPS chains were simplified to $-NH_2$ groups (which is equivalent to PAAm) to reduce the computational costs. The tensile force up to 4000 pico-Newton (i.e., $F_\tau = 4000$ pN), which is realized by our extended AFIR method,[31] is added diagonally to stretch both the polymer chain and the cross-linker molecule.[30] Our preliminary calculation results have suggested that the bond rupture occurs at the crosslinking area of the first network.[30] The possible force-induced bond cleavage sites, as well as the associated force-coupled free energy barriers $\Delta G_\tau^\ddagger$ at $F_\tau =$ 4000 pN, are shown in **Figure 2b** and **Figure S2-S4**. In the cases of the polymer networks synthesized with the crosslinkers MBAA and PEGDA, the most favored cleavage site is **A**, which subsequently generates two carbon-centered mechanoradicals. While for the polymer network synthesized with the crosslinker DVBS, the calculated cleavage site is **B**, which leads to a secondary carbon radical and a phenyl radical.

Having all these possible mechanoradicals located, we then explored the coupling reaction between them and the probe **P**. Gratifyingly, all the probe-radical coupling reactions were found having very little barrier or even barrierless (SI, **Figure S5-S9**), which ensures the proposed probing mechanism **1** shown in **Figure 1c**.

Considering the possible effect of oxygen on this type of reaction[33,34], further AFIR calculations revealed that it is also barrierless for the ground state triplet oxygen to be trapped by the mechanoradicals generated from the stretching process.[35-37] Shown in **Figure 3a**, it is clear that the addition of the first oxygen molecule to the carbon-centered radical **R1** is barrierless, and it subsequently generates a peroxide radical species **R2**. Meanwhile, the free energy is lowered by 52.9 $kJ \cdot mol^{-1}$ in association with this process. The formed peroxide radical **R2**, can immediately undergo an intramolecular C-H activation reaction by taking the hydrogen atom from either γ-, δ- or ε-carbon atom, as what can be seen in **Figure 3a**. Compared to the C-H activation at γ- and δ-position, the HAT (i.e., hydrogen atom transfer) reaction on the ε-carbon atom is energetically more favored, as the barrier is only +58.4 $kJ \cdot mol^{-1}$. The HAT reaction therefore offers another carbon-centered radical **R3**, which might directly react with the probe **P** via radical-radical coupling reaction to trigger the fluorescence. However, from another perspective, the newly formed ε-carbon radical **R3** can undergo further intramolecular radical reaction. For example, as shown in **Figure 3b**, the ε-carbon atom might attack the peroxide bond to furnish an intramolecular cyclisation and meanwhile release an OH radical (**Path A**). Alternatively, the ε-carbon atom can turn back and abstract the hydrogen atom from the α-carbon. The resultant α-carbon radical, which is directly connected to the peroxide moiety, is highly unstable and will immediately release an OH radical (**Path B**). According to the calculation results, both reactions were found highly exergonic. However, the former pathway has a free energy barrier lower than that of the latter. The effective barriers of **Path A** and **Path B** are +76.3 $kJ \cdot mol^{-1}$ (i.e., free energy gap between **R2** and **TS-3_6**) and +83.5 $kJ \cdot mol^{-1}$ (i.e., free energy barrier between **R2** and **TS-3_7**), respectively. Despite these two pathways discussed above, further calculation also revealed another reaction possibility called **Path C**, which involves two oxygen molecules as shown in **Figure 3b**. Instead of a direct intramolecular reaction from **R3**, due to the abundance of oxygen in the DN hydrogel system, the newly formed ε-carbon radical can interact with the second molecule of triplet oxygen, eventually introducing another peroxide bond to the ε-position. Compared to the first barrierless oxidation reaction, the second oxidation has a small barrier of +30.2 $kJ \cdot mol^{-1}$, probably because **R3** is a relatively stable tertiary carbon radical while **R1** is a secondary carbon radical. Moreover, in **R8**, the remaining C-H bond at the α-position can be subsequently activated by this newly generated peroxide bond, with an overall barrier of +60.6 $kJ \cdot mol^{-1}$ (i.e., corresponding to a $t_{1/2}$ of 4.62 ms, based on the Eyring equation). Similar to **Path A**, the HAT reaction generates an unstable α-carbon radical which will instantly decompose to render a ketone and an OH radical. The above DFT calculation results suggest that ·OH radicals can be readily generated within the timescale of several milliseconds.

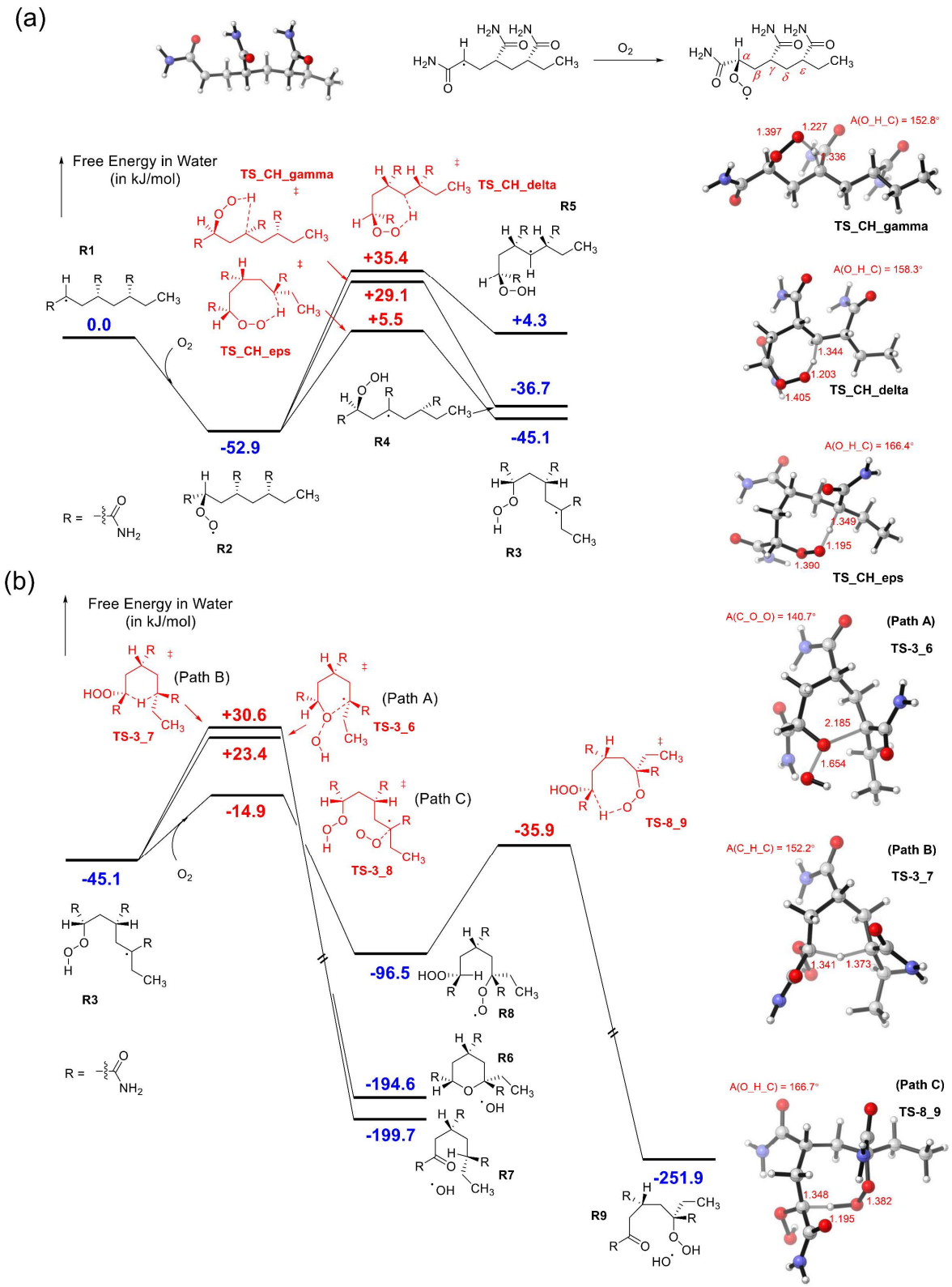

Figure 3. Computed reaction profile (UB3LYP-D3/Def2SVP level) for the generation of the hydroxyl radical from the reaction between mechanoradical and triplet O_2 molecule based on AFIR calculations. (a) Free energy profile for the intramolecular C-H activation of the mechanoradical at γ-, δ- and ε-position. Note that the newly formed C-O bond is very strong and the dissociation of C-O bond after the HAT reaction to generate an ·OOH radical is impossible. (b) Free energy profile for **Path A, B and C** based on the ε-carbon radical R3 and the subsequent formation of hydroxyl radical.

Grzybowski and co-workers have experimentally observed that the mechanoradicals in stressed dry polymer (e.g., PDMS and PVC) can react with the surrounding aqueous phase to generate H_2O_2 in water.[38] It was proposed that the mechanoradicals would generate OH radicals through reactions with oxygen, and these OH radicals would eventually produce H_2O_2.[38] Their pioneering work nicely supports our theoretical calculations on the generation of OH radicals (**Figure S10**). We have also computed the energy barrier for the formation of H_2O_2 from the different polymers (PAMPS in our case, PDMS and PVC in Grzybowski's work). The polymer used in our experiments, PAMPS, has the largest barrier of 102.8 kJ/mol (in comparison to the low barrier of 68.9 and 81.4 kJ/mol for PDMS and PVC, respectively), implying a very slow reaction for the generation of H_2O_2 from OH radicals under room temperature in our cases (**Figure S11**).

It is known that OH radical has a high mobility in the aqueous solution (with a diffusion coefficient of 2.8×10^{-5} cm^2/s and can rapidly diffuse via its huge hydrogen-bond network in water[39], **Figure S12**), and therefore can easily move around to trigger C-H activation reactions at rear and remote positions. Experimentally, it is expected that the probe **P** is strongly hydrophobic and meanwhile with an extremely low mobility in DN hydrogels, as it possesses a large coumarin-based group. Therefore, the probe **P** might adhere to somewhere along the polymer chain which is also hydrophobic. The formation of highly mobilized OH radical enables the C-H activation along the polymer chain, therefore greatly increasing the probability of coupling reaction between the probe and the carbon-centered radical (proposed oxygen-relayed mechanism **2** in **Figure 1c**). It is also confirmed by our DFT calculation that the direct coupling between OH radical and TEMPO moiety in probe **P** cannot compete with the coupling reaction between TEMPO and the carbon-centered radicals (supplementary text in SI, **Figure S13** and **S14**). Given these calculation results, the existence of oxygen does not terminate the mechanoradical species, but to relay the carbon-centered radical to the remote area so that the probability of the coupling reaction between the probe and the carbon-centered radical can be increased. These results strongly suggest the possibility of utilizing both probe **P** and oxygen for sensing and visualizing the mechanochemical damages in hydrogels on a real-time basis.

Mechanical behaviors of DN gels. DN hydrogels with distinctive mechanical behaviors are used in this study. The nominal stress σ-tensile strain ε curves for various DN virgin gels from **DN1** virgin to **DN5** virgin are shown in **Figure 4c**. In particular, **DN1**, **DN2** and **DN3** exhibit characteristic tensile curves for classical DN hydrogels[19, 40]: An abrupt stress decrease at a strain ε of 2.0, followed by a constant stress with the increase of strain from 2.0 to 10.0, and strain-hardening occurs at $\varepsilon > 10.0$ (**Figure 4a**). The constant stress regime above the yielding point is accompanied by the coexistence of necking region and unnecking region in the sample, and the necking region grows with the increase of strain, and develops to the whole sample at the point of strain-hardening. In the necking region, extensive internal fracturing of the brittle first network occurs, which generates a large amount of mechanoradicals, as illustrated in the molecular picture of the tensile process in **Figure 4b**.[20] **DN4** shows quite different tensile behaviors, such as no abrupt decrease in stress and a saturated plateau stress region in tensile curve. For **DN5**, it demonstrates an abrupt stress decrease phenomenon at an early ε of 1.2 and fractures at a low fracture strain of 3.5.

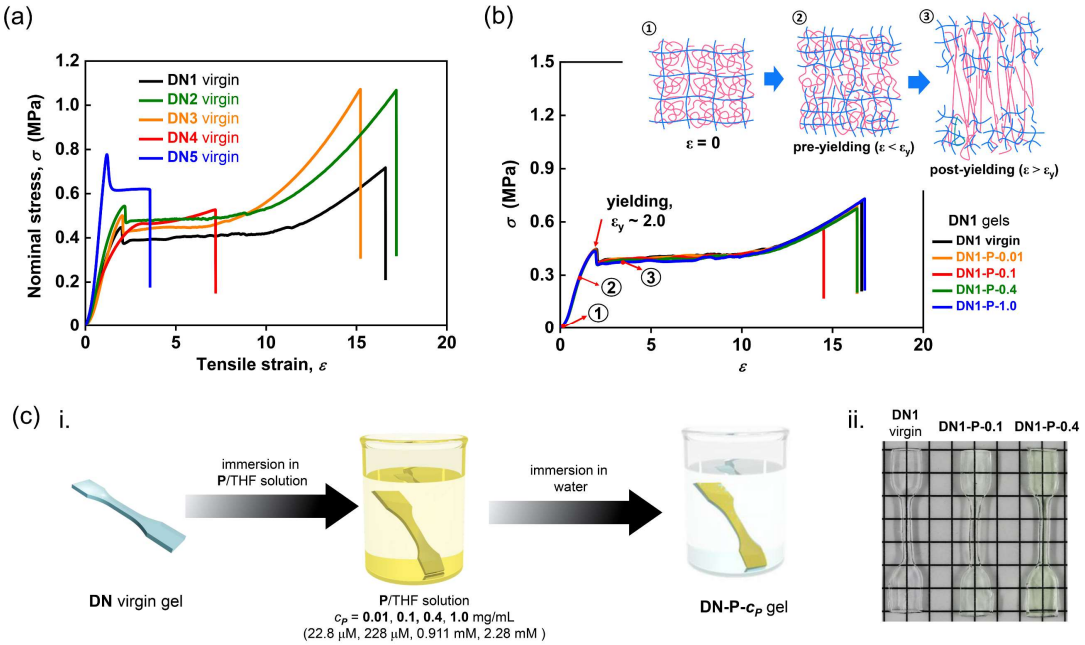

Figure 4. (a) The nominal stress σ-tensile strain ε curves for various DN virgin gels from **DN1** virgin to **DN5** virgin. (b) The nominal stress σ-tensile strain ε curves for **DN1** virgin and **DN1-P-c_p** gels with varied concentration c_p of prefluorescent reagent **P**. (c) Schematic illustration (i) of simple preparation of **DN-P-c_p** gels incorporated with prefluorescent reagent **P**. First, the virgin DN gels are immersed in **P**/THF solutions with various concentration c_p of **P** for 24 hours. Then, the DN gels are immersed into pure water to obtain the final **DN-P-c_p** gels. (ii) Photographs of **DN1** virgin, **DN1-P-0.1** and **DN1-P-0.4** gels.

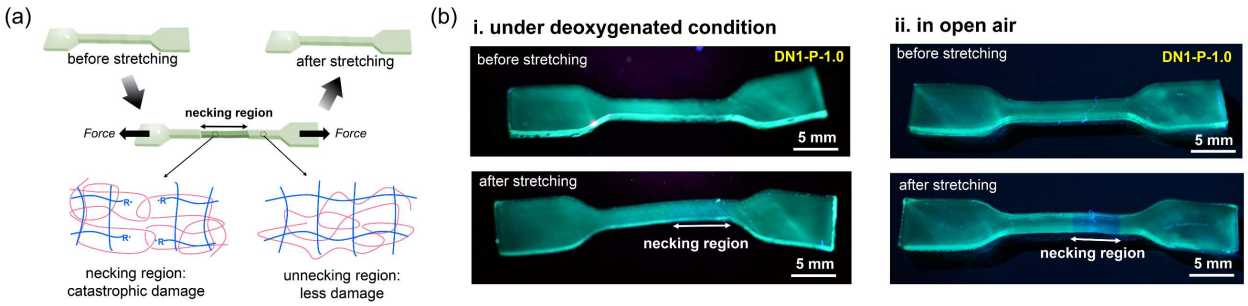

Figure 5. Oxygen-promoted mechano-responsive emission of the pre-fluorescence probe in the DN gel. (a) Schematic illustration of stretching-induced mechanochemical damages in DN gels. The necking region in DN gels shows catastrophic damage compared to unnecking region with less damage. (b) Photographs of **DN1-P-1.0** gel before and after stretching under deoxygenated condition (i) and in open air (ii) under UV light (λ_{ex} = 365 nm).

Post-loading of prefluorescent molecule P in DN gels. Different from the solid-state polymer powders which can be easily mixed with prefluorescent molecule **P**, it poses a great difficulty for the incorporation of the hydrophobic molecule **P** into DN hydrogels composed of hydrophilic polymer networks and a large amount of water (~ 90 wt%). To overcome this difficulty, we first dissolve the hydrophobic prefluorescent probe **P** in THF solvent to prepare the solution in different concentration c_P (0.01, 0.1, 0.4 and 1.0 mg/mL, corresponding to molar concentrations of 22.8 μM, 228 μM, 0.911 mM and 2.28 mM, respectively), and then immerse the DN virgin gels into the **P**/THF solutions for 24 hours. After that, the DN gels are directly immersed back into pure water, and the final gels are denoted as **DN-P-c_P** gels according to various concentration c_P (**Figure 4c(i)**). We next confirm that the probe **P** has been successfully incorporated into DN gels by this preparation protocol, and such a preparation process using **P**/THF solutions does not cause any damages to the final DN gels. We first show the behavior of **DN1** gels as a typical example. As shown in **Figure S15**, after immersion in **P**/THF solutions, the DN gels gradually shrink and become opaque, and the phase separation phenomenon occurs from sample edge to inside because THF is a relatively poor solvent for DN gels. After re-immersion into pure water, the DN gels are reswollen and recovered to their original shape with a slightly yellowish color, suggesting that prefluorescent probe **P** has been successfully incorporated into DN gels (**Figure 4c(ii)**). The high transparency and homogeneous appearance of the **DN-P-c_P** gels indicates that there is no probe aggregation occurring in the gel samples, therefore the probe molecules are expected to be well dispersed and sticked to the polymer chains. Moreover, the mechanical properties for **DN-P-c_P** gels with various c_P remained unchanged compared to the **DN** virgin gels (**Figure 4b**), and all the **DN** gels exhibit almost the same irreversible energy dissipation behaviors (SI, **Figure S16**), proving that such a preparation protocol using **P**/THF solutions does not cause any structure damages to the final DN gels. We also confirmed that other four types of DN gels, from **DN2** gels to **DN5** gels, also show the same behavior as **DN1** gels (SI, **Figure S17**).

Oxygen-promoted mechano-responsive emission of the pre-fluorescence probe in the DN gel media. Having successfully incorporated prefluorescent probe **P** into the DN gels, we next investigate whether the mechanochemical damages could be sensed or visualized by emission. As suggested by the theoretical calculations aforementioned, the oxygen may serve as a radical relayer to promote the mechanoradical probing. We first evaluate the role of oxygen on the mechanoradical probing by performing *in-situ* mechanochemical damage-sensing experiments on both deoxygenated DN gels and their counterparts in open air. We stretched the deoxygenated **DN1-P-1.0** gel and the one in open air to its necking regime by hand to ensure the generation of a large amount of mechanoradicals in the necking region, as illustrated in **Figure 5a**. The corresponding photographs before and after stretching for **DN1-P-1.0** gel under deoxygenated condition and in open air condition are shown in **Figure 5b**, respectively. As a first demonstration for the critical role that oxygen plays, the real-time process for **DN1-P-1.0** gel in open air under UV irradiation (λ_{ex}=365 nm) is also illustrated as a video clip in Supporting Movie S1, SI. Before stretching, the **DN1-P-1.0** gel exhibits a green emission under UV irradiation. Under stretching, **DN1-P-1.0** gel in open air immediately exhibits a dramatic change in photo emission from green to blue in the necking region where a large amount of mechanoradicals were generated. The blue emission remains even after the sample is unloading (**Figure 5b(ii)**). In contrast to the **DN1-P-1.0** gel in open air that shows clear emission change in necking region, the deoxygenated **DN1-P-1.0** gel only exhibits slight emission change in necking region (**Figure 5b(i)**). This result clearly confirms the significant role of oxygen in promoting mechanochemical damage-sensing, indicating that the reaction mechanism **2** plays a predominant role in comparison to reaction mechanism **1** under ambient conditions, which is consistent to the theoretical predictions.

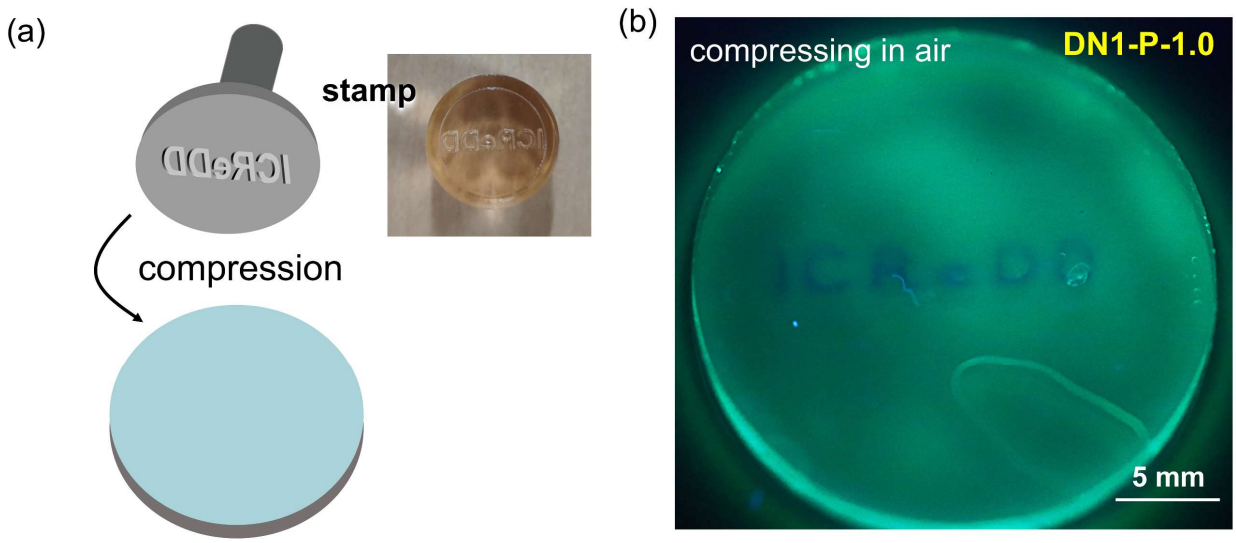

Figure 6. Visualization of compression-induced damages in DN gels using prefluorescent reagent **P.** (a) Illustration of compressing **DN1-P-1.0** gel using a stamp and (b) photograph showing the **DN1-P-1.0** gel after compression in air under UV light (λ_{ex} = 365 nm).

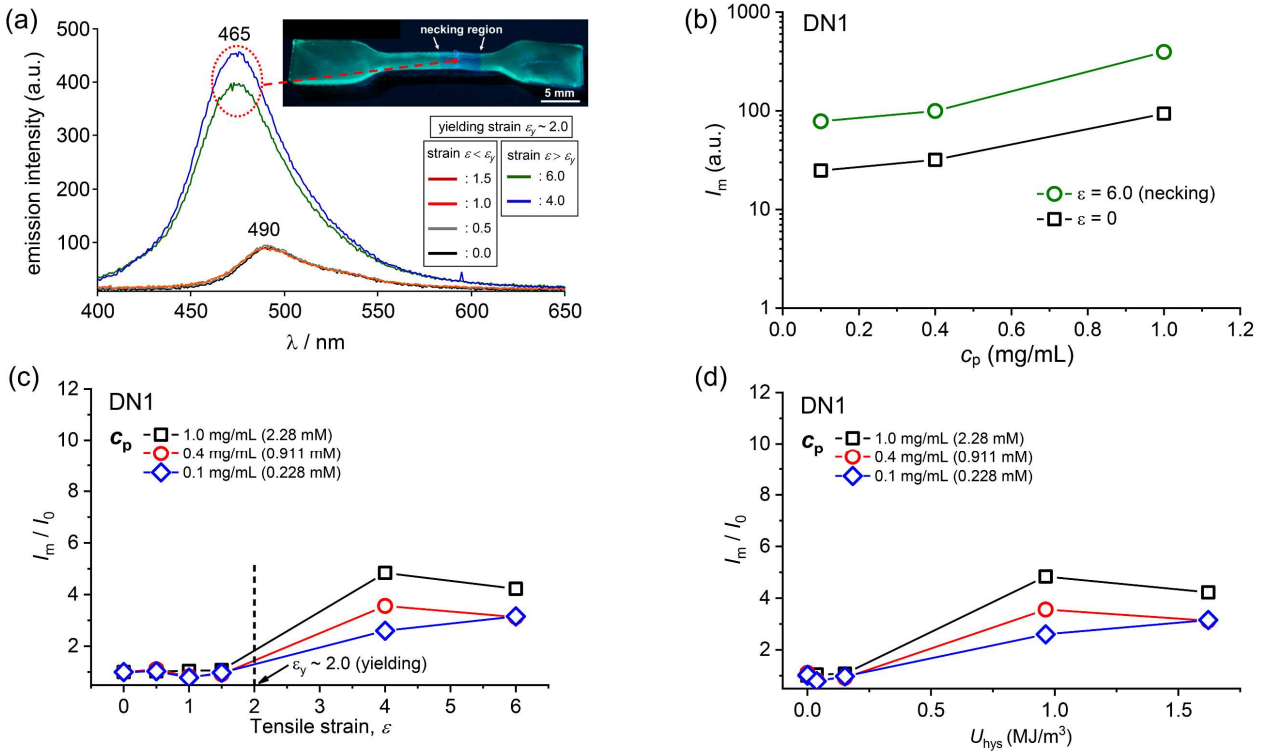

Figure 7. (a) Fluorescence spectra (λ_{ex} = 365 nm) of the **DN1-P-1.0** gels under various tensile strains. The fluorescence spectra at tensile strain of 4.0 and 6.0 are obtained in the necking region. (b) The peak emission intensity I_m from fluorescence spectra versus c_p at tensile strain of 6.0 and 0. (c) Emission intensity alternation ratio I_m/I_0 versus tensile strain ε and (d) I_m/I_0 versus hysteresis area U_{hys} for various **DN1-P-c_p** gels at different c_p. I_m and I_0 denote the peak intensity after stretching and before stretching, respectively.

The prefluorescent probe **P** could also visualize the compression-induced mechanochemical damage on a real-time basis. A **DN1-P-1.0** gel is compressed by a stamp embossed with the raised letters "ICReDD" (**Figure 6**) in open air. As shown in **Figure 6b**, after compression, the letters "ICReDD" with blue fluorescence emission under UV irradiation immediately appear in the stamped region. The spatial resolution of this method in sensing compression-induced mechanochemical damage is around 100 μm.

To further visualize the three-dimensional (3D) spatial mechanochemical damages, we adopted confocal laser scanning microscopy (CLSM). The excitation laser wavelength is λ_{ex} = 402.7 nm and the emission intensity is captured ranging from 451 to 471 nm. The 3D spatial visualizations of mechanochemical damages in stretched **DN1-P-1.0** gels are demonstrated in Supporting Movie S2 of SI. The representative snapshot of movie is shown in **Figure S18a**, SI. Note that these 3D images have been automatically constructed by the integration of a stack of scanned small original images captured by CLSM, which are shown as the mesh-like patterns in the integrated images. The weak intensity in the boundary area of these mesh-like patterns is caused by the CLSM microscope itself and therefore does not reveal any internal information. **DN1-P-1.0** gel exhibits the typical heterogeneous damage mode with clear and dramatic differences between necking region (severe damage) and unnecking region (weak damage), as illustrated in **Figure S18b**.[41] A typical CLSM image and the corresponding fluorescence intensity profile of the stretched **DN1-P-1.0** are shown in **Figures S18c** and **d**, respectively. The raw intensity data contain relatively strong noises, which may originate from experimental equipment such as from CLSM detector sensitivity and/or from the microscale inhomogeneity of the internal fracture. Hence, we also show moving-averaged data over 9 data points in **Figure S18d**, which gives an averaged value over a length scale of ~20 μm. The CLSM fluorescence intensity reflects the qualitative damage distribution because the damage-induced fluorescence emission shift will significantly increase the fluorescence intensity ranging from 451 - 471 nm. As shown in the fluorescence intensity profile in **Figures S18c** and **d**, **DN1-P-1.0** gel shows a dramatic and abrupt increase in the necking region compared to that in the unnecking region, which is in good agreement with our illustration on the heterogeneous damage mode (**Figure S18b**). The CLSM clearly shows a spatial resolution of 100 μm in the boundary of mechanochemical damage area, which is exactly the length scale of the transition zone between the necking and the unnecking regions in DN gels. It means that it is the substantial length scale of the damage transition zone, rather than our probe method, that determines the spatial resolution in detecting the mechanochemical damage in DN hydrogels. It thus suggests that our probe method has a much higher spatial resolution finer than 100 μm.

The blue emission shown in **Figure 5b** and **6b** should be originated from the fluorescence of the coumarin moiety in **P**, which is enhanced by the coupling reaction between generated mechanoradical in DN gels and free radical in TEMPO moiety in **P**, as reported in previous study,[24] which is in good agreement with our proposed mechanisms (**Figure 1c**). These results indicate that the prefluorescent molecule **P** can furnish the real-time sensing and visualization of the mechanochemical damages in hydrogels under ambient conditions with the presence of oxygen. We have also confirmed that the single network (SN) gels having the same compositions as in **DN1** gels show no emission change, since these SN gels can only generate a negligible number of mechano-radicals during deformation (**Figure S19**, SI)[20].

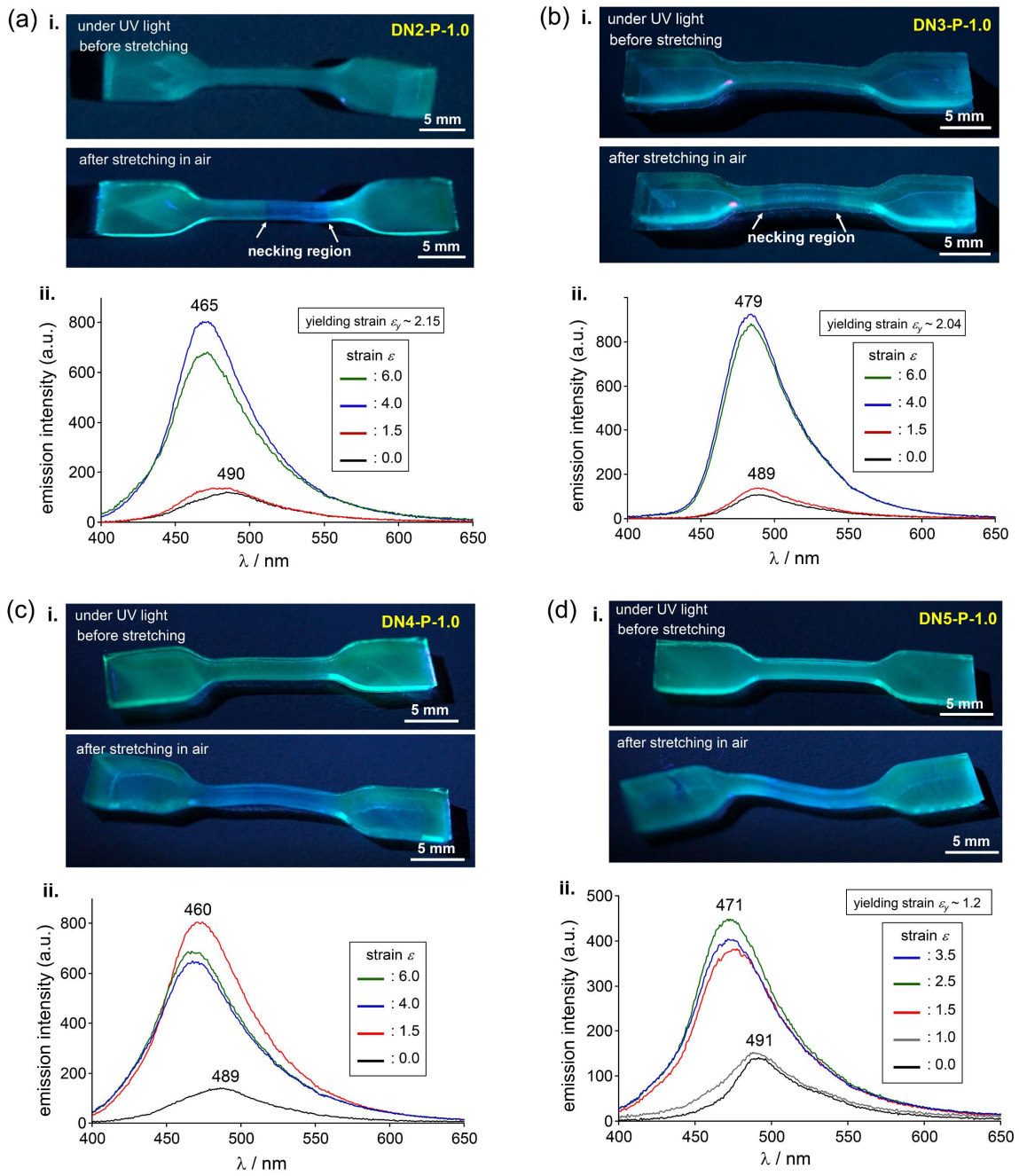

Figure 8. Photographs (i) before and after stretching in air under UV light (λ_{ex} = 365 nm), and fluorescence spectra (λ_{ex} = 365 nm) (ii) under various tensile strains for various **DN-P-c_P** gels: (a) **DN2-P-1.0**, (b) **DN3-P-1.0**, (c) **DN4-P-1.0**, (d) **DN5-P-1.0** gels.

We then systematically investigated the fluorescence spectra of **DN1-P-1.0** gel at a varied tensile strain using a tensile machine (**Figure 7a**). At the tensile strain of 0, the **DN1-P-1.0** gel shows green emission with a maximum emission-intensity at the wavelength ($\lambda_{em,max}$) of 490 nm. When the tensile strain is below the yielding strain ($\varepsilon < \varepsilon_y$), the fluorescence spectra hardly change. In contrast, with an increasing tensile strain beyond the yielding strain ($\varepsilon > \varepsilon_y$), the necking phase shows a blue fluorescence having $\lambda_{em,max}$ at 465 nm with ca. 4 times of emission enhancement from the unnecking phase. No distinct fluorescence emission change can be observed in the unnecking region. The fluorescence spectra hardly change with a strain above the yielding point for strain 4.0 and 6.0. This is because the increase of strain only increases the necking region fraction in the whole sample while the deformation of the necking region does not change above yielding point. As the internal rupture of the first network occurs even before yielding but with less significance[41], the results indicates that **P** is not sensitive enough to probe the pre-yielding damage.

To investigate the sensitivity of the probe, we investigated the effect of the in-feed concentration c_P of the pre-fluorescence probe **P** to the mechano-responsive emission of **DN1-P-c_P** gels.

We observed that the gel prepared by using low concentration of the **P**/THF solution [0.01 mg/mL (22.8 μM)] showed very week emission, allowing no further evaluation via the emission change (**Figure S20-S24**).[42] On the other hand, the DN gels prepared by the **P**/THF solution having relatively higher concentration of **P** ranging from 0.1 to 1.0 mg/mL (228 μM to 2.28 mM) exhibited the clear emission enhancement by the mechanical stress that induced the gel deformation (**Figure 5b** and **S20-S24**). The emission intensity after stretching (ε = 6.0) and before stretching (ε = 0) increases with the in-feed probe concentration c_P (**Figure 7b**). This result indicates that the concentration of probe **P** included in the DN gel increases with a rising c_P. To evaluate if the relative blue emission intensity is independent of c_P in the investigated range, we plotted the emission intensity ratio after and before stretching, I_m/I_0, as a function of the tensile strain ε in **Figures 7c**, where I_m and I_0 denote the peak emission intensity after stretching and before stretching, respectively. Although the absolute emission intensity increases with c_P, the ratio I_m/I_0 hardly changes with c_P and increases with tensile strain ε (**Figure 7c** and **S25**). When tensile strain is below yielding strain ($\varepsilon < \varepsilon_y$), I_m/I_0 is nearly identical to 1.0, indicating a negligible mechanoradical generation. In contrast, when the tensile strain is increased beyond the yielding ($\varepsilon > \varepsilon_y = 2.0$), I_m/I_0 abruptly increases, indicating a remarkable mechanoradical generation.

As clarified in the previous works, the mechanochemical damage dissipates a large amount of energy, and the dissipated energy U_{hys} can be estimated from the mechanical hysteresis loop (SI). As the dissipated energy U_{hys} should be entirely consumed in the bond scissions of the first network strands, the concentration of mechanoradicals C_{rad} should be proportional to the dissipated energy. So we further plot I_m/I_0 as a function of dissipated energy U_{hys} in **Figure 7d**. We clearly see that I_m/I_0 increases with U_{hys} up to the yielding of the sample and then almost unchanged. This is again because once above yielding, the increase of U_{hys} is due to the increase of the necking zone fraction in the whole sample while the degree of mechanochemical damage of the necking region does not change above the yielding point.

As elucidated in the previous studies, the mechanoradical concentration in the necking region in conventional DN hydrogels crosslinked by MBAA is in the order of 10 μM while the mechanoradicals generated in the unnecking region may be one order lower.[20] Since we only observed clear fluorescence emission change in the necking region rather than the unnecking region, the concentration resolution of our probe should be around several μM. This resolution is high comparing with the diarylacetonitrile probe that showed a resolution to ~10^{-5} mmol radicals in 50 mg polystyrene powder, corresponding to a concentration resolution of ~mM.[22]

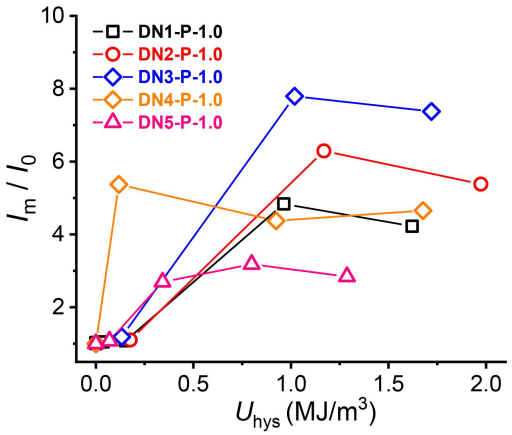

Figure 9. Emission intensity alternation ratio I_m/I_0 versus hysteresis area U_{hys} for various **DN-P-1.0** gels.

Generality of the pre-fluorescent probe in various DN gel media. To confirm the generality of this method, we further performed the real-time visualization of internal damages with other four types of DN gels. Specifically, **DN2** to **DN5** gels prepared from varied monomers and crosslinkers were tested. The real-time visualization of the stretching-induced damages for **DN2-P-1.0**, **DN3-P-1.0**, **DN4-P-1.0** and **DN5-P-1.0** gels are also demonstrated in Supporting Movie S1, SI, and the corresponding photographs before and after stretching are shown in **Figure 8**. As exhibited by their tensile curves (**Figure 4a**), **DN2-P-1.0** and **DN3-P-1.0** gels show similar characteristic tensile behaviors, such as the abrupt stress-yielding and the subsequent necking expansion phenomena, which were also observed for **DN1-P-1.0** gel. Thus, **DN2-P-1.0** and **DN3-P-1.0** gels also exhibit a dramatic fluorescence emission change from green to blue color in the necking region where massive mechanoradicals were generated from extensive fracturing of stiff and brittle first network strands like **DN1-P-1.0** gel. Different from **DN1-P-1.0**, **DN2-P-1.0** and **DN3-P-1.0** gels, which showed a clear emission in the necking area, **DN4-P-1.0** gel demonstrates a saturated plateau stress region where the sample deforms homogeneously without showing the necking behavior.[43] The supporting Movie S1 of SI and **Figure 8c** strongly indicate that the whole deformed region of **DN4-P-1.0** gel homogeneously emits blue fluorescence, suggesting that the whole deformed region homogeneously generates sufficient and tremendous amounts of mechanoradicals to react with **P,** thus allowing the emission of a strong blue fluorescence. **DN5-P-1.0** gel also demonstrates quite different tensile behaviors with an abrupt stress-yielding phenomenon at an early ε of 1.2, and the multi-necking occurs simultaneously in the deformed region, showing a dramatic blue fluorescence change (Supporting Movie S1, SI). The detailed fluorescence measurements for **DN2-P-1.0**, **DN3-P-1.0**, **DN4-P-1.0** and **DN5-P-1.0** gels under various tensile strains are systematically conducted, and the corresponding fluorescence emission spectra are shown in (ii) of **Figure 8(a-d)**, respectively. The emission enhancement with the blue-shifted emission spectra is clearly observed when the DN gels were deformed by the mechanical stress that is larger than the yielding strain for the necking event. These observations are consistent with our DFT calculation results as mentioned previously. It clearly indicated that the free-radical in the probe **P** can react in barrierless with the generated mechanoradicals in the cleaved polymer networks among different DN gels (**Figure S5-S9**).

Moreover, we also evaluated emission intensity ratio I_m/I_0 for different DN gels and plotted the data against the dissipated energy U_{hys} in **Figure 9**. We found that among these five types of DN gels, **DN4** stands out with the highest sensitivity to a small dissipation energy of only 0.11 MJ/m^3. Given the fact that these five types of DN all have comparable Young's modulus (**Figure 4a**), **DN4** should have a comparable amount of strand density with other kinds of DN gels. The high sensitivity of **DN4** indicates that the **P** probe might have a high efficiency to react with the mechanoradicals of DVBS crosslinkers. This is possibly due to the similar hydrophobic structure between coumarin-based probe **P** and benzene ring in DVBS crosslinkers, making the probe **P** distributed near DVBS crosslinking points. Once sufficient amount of mechanoradicals were generated from DVBS crosslinking points, these mechanoradicals can be immediately trapped by probe **P**.

3. Conclusions

Herein, we have succeeded in proving the possibility of using the prefluorescent molecule **P**, which possesses a coumarin-based luminophore with a TEMPO moiety that contains free radical, for the real-time sensing and visualization of mechanochemical damages in DN hydrogels. The theoretical calculations do not only confirm the barrierless coupling reaction between **P** and mechanoradicals in DN gels, but also suggest an oxygen-relayed radical transfer mechanism in promoting the probability of the coupling reaction between the probe **P** and radicals originally from the mechanochemical reactions. By pre-loading the prefluorescent molecule **P** into DN gels, the severely damaged region by mechanical stretching and compression immediately exhibits a dramatically enhanced emission in open air, in accompany with a change of color from green to blue. It is caused by the oxygen-relayed radical transfer process and the coupling reaction of radicals in DN gels with the free radical of the TEMPO moiety in **P.** It should be emphasized that, this method which utilizes a prefluorescent molecule probe is simple but meanwhile reliable. There is no need for incorporating the mechanophore into the polymer backbone, which does not change the original network structure so that the original material properties could be kept. Furthermore, this method developed by us has advantages to easily achieve *in-situ* and real-time observation under ambient conditions with the presence of oxygen.[17] Moreover, to the best of our knowledge, this work presented here is the first report utilizing oxygen as a radical relayer for visualizing mechanoradical damages in polymer materials.

ASSOCIATED CONTENT

Supporting information. Details of reagents used, hydrogel synthesis procedure and the computational simulation, procedure of the prefluorescent molecule **P** treatment to hydrogel, mechanical tests, fluorescence measurements, spatial visualization by CLSM and DFT calculations for the probe-radical coupling reaction.

AUTHOR INFORMATION

Corresponding Authors

*Mingoo Jin - Institute for Chemical Reaction Design and Discovery (WPI-ICReDD), Hokkaido University, Sapporo 001-0021, Japan; Division of Applied Chemistry, Graduate School of Engineering, Hokkaido University, Sapporo, 060-8628, Japan; E-mail: mingoo@icredd.hokudai.ac.jp

*Satoshi Maeda - Institute for Chemical Reaction Design and Discovery (WPI-ICReDD), Hokkaido University, Sapporo 001-0021, Japan; Department of Chemistry, Faculty of Science, Hokkaido University, Sapporo, 060-8628, Japan;
Email: smaeda@eis.hokudai.ac.jp

*Hajime Ito - Institute for Chemical Reaction Design and Discovery (WPI-ICReDD), Hokkaido University, Sapporo 001-0021, Japan; Division of Applied Chemistry, Graduate School of Engineering, Hokkaido University, Sapporo, 060-8628, Japan;
Email: hajito@eng.hokudai.ac.jp

*Jian Ping Gong - Institute for Chemical Reaction Design and Discovery (WPI-ICReDD), Hokkaido University, Sapporo 001-0021, Japan; Faculty of Advanced Life Science, Hokkaido University, Sapporo 001-0021, Japan;
E-mail: gong@sci.hokudai.ac.jp

Authors

Yong Zheng - Institute for Chemical Reaction Design and Discovery (WPI-ICReDD), Hokkaido University, Sapporo 001-0021, Japan.

Julong Jiang - Department of Chemistry, Faculty of Science, Hokkaido University, Sapporo, 060-8628, Japan.

Daiyo Miura - Division of Applied Chemistry, Graduate School of Engineering, Hokkaido University, Sapporo 060-8628 Japan.

Fei Xue Lu - Graduate School of Life Science, Hokkaido University, Sapporo 001-0021, Japan.

Koji Kubota - Institute for Chemical Reaction Design and Discovery (WPI-ICReDD), Hokkaido University, Sapporo 001-0021, Japan; Division of Applied Chemistry, Graduate School of Engineering, Hokkaido University, Sapporo, 060-8628, Japan.

Tasuku Nakajima - Institute for Chemical Reaction Design and Discovery (WPI-ICReDD), Hokkaido University, Sapporo 001-0021, Japan; Faculty of Advanced Life Science, Hokkaido University, Sapporo 001-0021, Japan.

Author Contributions

The manuscript was written through contributions of all authors. All authors have given approval to the final version of the manuscript. ‡Y.Z. and J.J. contributed equally to this work.

Notes

ORCIDs of the authors
Yong Zheng: 0000-0002-9445-1229
Mingoo Jin: 0000-0001-6199-8802
Fei Xue Lu: 0000-0001-7133-273X
Koji Kubota: 0000-0003-1522-291X
Tasuku Nakajima: 0000-0002-2235-3478
Satoshi Maeda: 0000-0001-8822-1147
Hajime Ito: 0000-0003-3852-6721
Jian Ping Gong: 0000-0003-2228-2750

ACKNOWLEDGMENT

This work was financially supported by the Japan Society for the Promotion of Science (JSPS) via KAKENHI grants JP17H06370, JP17H06144, JP18H03907, JP21K14637, JP22K18333, JP22H00318, JP22H04968, and JP22K21342; by the JST via FOREST grant JPMJFR201I, CREST grant JPMJCR19R1 and ERATO grant JPMJER1903; and by the Institute for Chemical Reaction Design and Discovery (ICReDD), established by the World Premier International Research Initiative (WPI), MEXT, Japan. The authors thank Tosoh Finechem Corporation for providing DVBS. Y.Z. is grateful to the Nikon Imaging Center at Hokkaido University and Kentaro Kobayashi for his help with confocal microscopy, image acquisition, and analysis, and Qifeng Mu for

preparation of 3D-printed stamp embossed with the raised letters "ICReDD".

REFERENCES

(1) Slootman, J.; Waltz, V.; Yeh, C. J.; Baumann, C.; Göstl, R.; Comtet, J.; Creton, C. Quantifying rate-and temperature-dependent molecular damage in elastomer fracture. *Phys. Rev. X.* **2020,** 10, 041045.

(2) Slootman, J.; Yeh, C. J.; Millereau, P.; Comtet, J.; Creton, C. A molecular interpretation of the toughness of multiple network elastomers at high temperature. *Proc. Natl. Acad. Sci. U.S.A.* **2022,** 119, e2116127119.

(3) Imato, K.; Kanehara, T.; Ohishi, T.; Nishihara, M.; Yajima, H.; Ito, M.; Takahara, A.; Otsuka, H. Mechanochromic dynamic covalent elastomers: quantitative stress evaluation and autonomous recovery. *ACS Macro Lett.* **2015,** 4, 1307-1311.

(4) Sakai, H.; Aoki, D.; Seshimo, K.; Mayumi, K.; Nishitsuji, S.; Kurose, T.; Ito, H.; Otsuka, H. Visualization and quantitative evaluation of toughening polymer networks by a sacrificial dynamic crosslinker with mechanochromic properties. *ACS Macro Lett.* **2020**, 9, 1108-1113.

(5) Ishizuki, K.; Aoki, D.; Goseki, R.; Otsuka, H. Multicolor mechanochromic polymer blends that can discriminate between stretching and grinding. *ACS Macro Lett.* **2018,** 7, 556-560.

(6) Ducrot, E.; Chen, Y.; Bulters, M.; Sijbesma, R. P.; Creton, C. Toughening elastomers with sacrificial bonds and watching them break. *Science* **2014,** 344, 186-189.

(7) Chen, Y.; Mellot, G.; van Luijk, D.; Creton, C.; Sijbesma, R. P. Mechanochemical tools for polymer materials. *Chem. Soc. Rev.* **2021,** 50, 4100-4140.

(8) Wang, S.; Beech, H. K.; Bowser, B. H.; Kouznetsova, T. B.; Olsen, B. D.; Rubinstein, M.; Craig, S. L. Mecha-nism dictates mechanics: a molecular substituent effect in the macroscopic fracture of a covalent polymer network. *J. Am. Chem. Soc.* **2021**, 143, 3714-3718.

(9) Wang, Z.; Zheng, X.; Ouchi, T.; Kouznetsova, T. B.; Beech, H. K.; Av-Ron, S.; Matsuda, T.; Bowser, B. H.; Wang, S.; Johnson, J. A. Toughening hydrogels through force-triggered chemical reactions that lengthen polymer strands. *Science* **2021**, 374, 193-196.

(10) Watabe, T.; Aoki, D.; Otsuka, H. Polymer-Network Toughening and Highly Sensitive Mechanochromism via a Dynamic Covalent Mechanophore and a Multinetwork Strategy. *Macromolecules* **2022**, 55, 5795-5802.

(11) Boulatov, R., *Polymer Mechanochemistry*. Springer: **2015**; Vol. 369; pp 209–238.

(12) Kuzuya, M.; Kondo, S. I.; Noguchi, A.; Noda, N. Nature of mechanoradical formation and reactivity with oxygen in methacrylic vinyl polymers. *J. Polym. Sci. B: Polym. Phys.* **1992**, 30, 97-103.

(13) Beyer, M. K.; Clausen-Schaumann, H. Mechanochemistry: the mechanical activation of covalent bonds. *Chem. Rev.* **2005**, 105, 2921-2948.

(14) Kawashima, T.; Shimada, S.; Kashiwabara, H.; Sohma, J. ESR studies on the molecular mechanisms of fracture of polymers at low temperatures. *Polym. J.* **1973,** 5, 135-143.

(15) Sakaguchi, M.; Sohma, J. ESR evidence for main-chain scission produced by mechanical fracture of polymers at low temperature. *J. Polym. Sci., Part B: Polym. Phys.* **1975,** *13*, 1233-1245.

(16) Tabata, M.; Yamakawa, H.; Takahashi, K.; Sohma, J. ESR studies on the conversion of mechanoradicals of poly (methyl methacrylate) and its self-degradation. *Polym. Degrad. Stab.* **1979**, 1, 57-68.

(17) Matsuda, T.; Kawakami, R.; Nakajima, T.; Gong, J. P. Crack Tip Field of a Double-Network Gel: Visualization of Covalent Bond Scission through Mechanoradical Polymerization. *Macromolecules* **2020,** 53, 8787-8795.

(18) Gong, J. P.; Katsuyama, Y.; Kurokawa, T.; Osada, Y. Double-network hydrogels with extremely high mechanical strength. *Adv. Mater.* **2003,** 15, 1155-1158.

(19) Gong, J. P. Why are double network hydrogels so tough? *Soft Matter* **2010,** 6, 2583-2590.

(20) Matsuda, T.; Kawakami, R.; Namba, R.; Nakajima, T.; Gong, J. P. Mechanoresponsive self-growing hydrogels inspired by muscle training. *Science* **2019,** 363, 504-508.

(21) Forstner, H.; Gnaiger, E. *Calculation of Equilibrium Oxygen Concentration*. Springer, Berlin, Heidelberg. 1983; pp 321-333.

(22) Yamamoto, T.; Kato, S.; Aoki, D.; Otsuka, H. A Diarylacetonitrile as a Molecular Probe for the Detection of Polymeric Mechanoradicals in the Bulk State through a Radical Chain-Transfer Mechanism. *Angew. Chem.* **2021,** 133, 2712-2715.

(23) Wang, F.; Burck, M.; Diesendruck, C. E. Following homolytic mechanochemical kinetics with a pyrenyl nitrone spin trap. *ACS Macro Lett.* **2017**, 6, 42-45.

(24) Kubota, K.; Toyoshima, N.; Miura, D.; Jiang, J.; Maeda, S.; Jin, M.; Ito, H. Introduction of a Luminophore into Generic Polymers via Mechanoradical Coupling with a Prefluorescent Reagent. *Angew. Chem.* **2021**, 133, 16139-16144.

(25) Green, S.; Simpson, D.; Zhou, G.; Ho, P.; Blough, N. V. Intramolecular quenching of excited singlet states by stable nitroxyl radicals. *J. Am. Chem. Soc.* **1990,** 112, 7337-7346.

(26) Silaev, M. Simulation of the initiated addition of hydrocarbon free radicals and hydrogen atoms to oxygen via a nonbranched chain mechanism. *Theor. Found. Chem. Eng.* **2007**, 41, 831-838.

(27) Wang, J.; Kouznetsova, T. B.; Craig, S. L. Single-molecule observation of a mechanically activated cis-to-trans cyclopropane isomerization. *J. Am. Chem. Soc.* **2016**, 138, 10410-10412.

(28) Simic, M. G. Free radical mechanisms in autoxidation processes. *J. Chem. Educ.* 1981, 58, 125.

(29) Parkatzidis, K.; Truong, N. P.; Whitfield, R.; Campi, C. E.; Grimm-Lebsanft, B.; Buchenau, S.; Rübhausen, M. A.; Harrisson, S.; Konkolewicz, D.; Schindler, S; Anastasaki, A. Oxygen-Enhanced Atom Transfer Radical Polymerization through the Formation of a Copper Superoxido Complex. *J. Am. Chem. Soc.* **2023**, 145, 1906–1915.

(30) Wang, Z.; Jiang, J.; Mu, Q.; Maeda, S.; Nakajima, T.; Gong, J. P. *J. Am. Chem. Soc.* **2022**, 144, 3154-3161.

(31) (a) Maeda, S.; Ohno, K.; Morokuma, K. Systematic exploration of the mechanism of chemical reactions: the global reaction route mapping (GRRM) strategy using the ADDF and AFIR methods. *Phys. Chem. Chem. Phys.* **2013**, 15, 3683-3701. (b) Maeda, S.; Harabuchi, Y.; Takagi, M.; Taketsugu, T.; Morokuma, K. Artificial force induced reaction (AFIR) method for exploring quantum chemical potential energy surfaces. *Chem. Rec.* **2016**, 16, 2232-2248. (c) Maeda, S.; Harabuchi, Y.; Takagi, M.; Saita, K.; Suzuki, K.; Ichino, T.; Sumiya, Y.; Sugiyama, K.; Ono, Y. *J.* Implementation and performance of the artificial force induced reaction method in the GRRM17 program. *Comput. Chem.* **2018**, 39, 233-251. (d) Hatanaka, M.; Yoshimura, T.; Maeda, S. Artificial force-induced reaction method for systematic elucidation of mechanism and selectivity in organometallic reactions. *Top. Organomet. Chem.* **2020**, 67, 57-80. (e) Maeda, S.; Harabuchi, Y. Exploring paths of chemical transformations in molecular and periodic systems: An approach utilizing force. *WIREs Comput. Mol. Sci.* **2021**, 11, e1538.

(32) Jiang, J.; Kubota, K.; Jin, M.; Wang, Z.; Nakajima, T.; Ito, H; Gong, J. P; Maeda, S. Computational Exploration of Polymer Mechanochemistry: Quantitation of Activation Force and Systematic Discovery of Reaction Sites Utilizing Two Forces. *ChemRxiv.* **2022**. DOI: 10.26434/chemrxiv-2022-fr09l. (accessed 2023-02-22)

(33) Tokmakov, I.; Kim, G.; Kislov, V; Mebel, A; Lin, M. The reaction of phenyl radical with molecular oxygen: A G2M study of the potential energy surface. *J. Phys. Chem. A*, **2005**, 109, 6114-6127.

(34) Du, H.; Gong, X. A theoretical study on the reaction mechanism of O2 with C4H9• radical. *J. Mol. Model.*, **2012**, 18, 2219-2226.

(35) da Silva, G.; Chen, C.-C.; Bozzelli, J. W. Toluene combustion: reaction paths, thermochemical properties, and kinetic analysis for the methylphenyl radical+ O2 reaction. *J. Phys. Chem. A.* **2007,** 111, 8663-8676.

(36) Prendergast, M. B.; Cooper, P. A.; Kirk, B. B.; da Silva, G.; Blanksby, S. J.; Trevitt, A. J. Hydroxyl radical formation in the gas phase oxidation of distonic 2-methylphenyl radical cations. *Phys. Chem. Chem. Phys.* **2013,** 15, 20577-20584.

(37) Prendergast, M. B.; Kirk, B. B.; Savee, J. D.; Osborn, D. L.; Taatjes, C. A.; Masters, K.-S.; Blanksby, S. J.; Da Silva, G.; Trevitt, A.

J. Formation and stability of gas-phase o-benzoquinone from oxidation of ortho-hydroxyphenyl: a combined neutral and distonic radical study. *Phys. Chem. Chem. Phys.* **2016,** 18, 4320-4332.

(38) Baytekin, H. T.; Baytekin, B.; Grzybowski, B. A. Mechanoradicals created in "polymeric sponges" drive reactions in aqueous media. *Angew. Chem.* **2012**, 51, 3596-3600.

(39) Codorniu-Hernández, E.; Kusalik, P. G. Mobility mechanism of hydroxyl radicals in aqueous solution via hydrogen transfer. *J. Am. Chem. Soc.* **2012,** 134, 532-538.

(40) Nakajima, T.; Kurokawa, T.; Ahmed, S.; Wu, W.-l.; Gong, J. P. Characterization of internal fracture process of double network hydrogels under uniaxial elongation. *Soft Matter* **2013,** 9, 1955-1966.

(41) Matsuda, T.; Kawakami, R.; Nakajima, T.; Hane, Y.; Gong, J. P. Revisiting the Origins of the Fracture Energy of Tough Double-Network Hydrogels with Quantitative Mechanochemical Characterization of the Damage Zone. *Macromolecules* **2021,** 54, 10331-10339.

(42) For the DN1-P-0.01, the emission was too weak to be measured by the fluorometer.

(43) Fukao, K.; Nakajima, T.; Nonoyama, T.; Kurokawa, T.; Kawai, T.; Gong, J. P. Effect of Relative Strength of Two Networks on the Internal Fracture Process of Double Network Hydrogels As Revealed by in Situ Small-Angle X-ray Scattering. *Macromolecules* **2020,** 53, 1154-1163.

SYNOPSIS TOC